Monthly Notices of the ROYAL ASTRONOMICAL SOCIETY

MNRAS **443,** 1211–1223 (2014) doi:10.1093/mnras/stu1193

Decoding the X-ray properties of pre-reionization era sources

Jordan Mirocha*

Center for Astrophysics and Space Astronomy and Department of Astrophysical and Planetary Science, University of Colorado, Campus Box 389, Boulder, CO 80309, USA

Accepted 2014 June 16. Received 2014 June 7; in original form 2014 April 5

ABSTRACT

Evolution in the X-ray luminosity–star formation rate ($L_{\rm X}$–SFR) relation could provide the first evidence of a top-heavy stellar initial mass function in the early Universe, as the abundance of high-mass stars and binary systems are both expected to increase with decreasing metallicity. The sky-averaged (global) 21-cm signal has the potential to test this prediction via constraints on the thermal history of the intergalactic medium, since X-rays can most easily escape galaxies and heat gas on large scales. A significant complication in the interpretation of upcoming 21-cm measurements is the unknown spectrum of accreting black holes (BHs) at high-z, which depends on the mass of accreting objects and poorly constrained processes such as how accretion disc photons are processed by the disc atmosphere and host galaxy interstellar medium. Using a novel approach to solving the cosmological radiative transfer equation (RTE), we show that reasonable changes in the characteristic BH mass affects the amplitude of the 21-cm signal's minimum at the ~10–20 mK level – comparable to errors induced by commonly used approximations to the RTE – while modifications to the intrinsic disc spectrum due to Compton scattering (bound-free absorption) can shift the position of the minimum of the global signal by $\Delta z \approx 0.5$ ($\Delta z \approx 2$), and modify its amplitude by up to ≈10 mK (≈50 mK) for a given accretion history. Such deviations are larger than the uncertainties expected of current global 21-cm signal extraction algorithms, and could easily be confused with evolution in the $L_{\rm X}$–SFR relation.

Key words: methods: numerical – dark ages, reionization, first stars – diffuse radiation – X-rays: binaries – X-rays: diffuse background.

1 INTRODUCTION

The Universe's transition from a cold and mostly neutral state after cosmological recombination, to a hot, ionized plasma, ~1 billion years later, encodes information about the first generations of stars, galaxies, and compact objects (Barkana & Loeb 2001; Bromm et al. 2009). However, two major astrophysical milestones are likely to occur well before this Epoch of Reionization (EoR) began in earnest, which are both valuable probes of the high-redshift Universe: (1) decoupling of the excitation temperature of ambient intergalactic hydrogen gas from the cosmic microwave background (CMB) temperature by a soft ultraviolet background (Wouthuysen 1952; Field 1958; Madau, Meiksin & Rees 1997; Barkana & Loeb 2005), and (2) X-ray heating of the intergalactic medium (IGM), eventually to temperatures above the CMB temperature (Venkatesan et al. 2001; Chen & Miralda-Escudé 2004; Madau et al. 2004; Ricotti & Ostriker 2004; Ciardi, Salvaterra & Di Matteo 2010; Mcquinn 2012). These events are expected to be visible in absorption against the CMB at low radio frequencies, $\nu = \nu_0(1 + z)$, where $\nu_0 = 1420$ MHz is the rest frequency of the ground-state hyperfine 21-cm transition of neutral hydrogen, and z is the redshift (for a review, see Furlanetto, Oh & Briggs 2006).

Studies of the pre-reionization epoch via the redshifted 21-cm line in absorption have the potential to provide the first contemporaneous constraints on the properties of the first stars and black holes (BHs), whose formation channels may be fundamentally different than those of their counterparts in the local Universe (e.g. Bromm, Coppi & Larson 1999; Abel, Bryan & Norman 2002; Begelman, Volonteri & Rees 2006). Their existence could dramatically alter the conditions for subsequent star and BH formation in their host haloes, and perhaps globally, through strong photodissociating and photoionizing radiation (e.g. Haiman, Abel & Rees 2000; Kuhlen & Madau 2005; Mesinger, Bryan & Haiman 2009; Tanaka, Perna & Haiman 2012; Wolcott-Green & Haiman 2012; Jeon et al. 2014).

In this work, we focus on the minimum of the global 21-cm signal and how its position could be used to probe the properties of accreting BHs in the early Universe. The 21-cm minimum is well known as an indicator of heating (e.g. Furlanetto 2006; Pritchard & Furlanetto 2007; Mirabel et al. 2011), and from its position one can obtain model-independent limits on the instantaneous heating rate density and cumulative heating in the IGM over time (Mirocha,

*E-mail: jordan.mirocha@colorado.edu

Harker & Burns 2013). The 21-cm maximum is also a probe of the IGM thermal history (e.g. Ripamonti, Mapelli & Zaroubi 2008), though because it likely overlaps with the early stages of reionization, one must obtain an independent measurement on the ionization history in order to constrain the IGM temperature and heating rate density (Mirocha et al. 2013). In either case, extracting the properties of the heat sources themselves from the 21-cm signal is fraught with uncertainty since the number density of X-ray sources and their individual luminosities cannot be constrained independently by volume-averaged measures like the global 21-cm signal.

Despite such degeneracies among model parameters, accurate enough measurements could still rule out vast expanses of a currently wide-open parameter space. What remains could be visualized as a two-dimensional posterior probability distribution that characterizes the likelihood that any given pair of model parameters is correct, having marginalized over uncertainties in all additional parameters. Two likely axes in such analyses include (1) the characteristic mass (or virial temperature) of star-forming haloes and (2) the X-ray luminosity per unit star formation. However, a third, and often ignored axis that will manifest itself in such posterior probability spaces is the spectral energy distribution (SED) of X-ray sources. The reason for this expectation is simple: soft X-ray sources will heat the IGM more efficiently than hard X-ray sources (at fixed total X-ray luminosity) due to the strong frequency dependence of the bound-free absorption cross-section ($\sigma \propto \nu^{-3}$ approximately).

High-mass X-ray binaries (HMXBs) are often assumed to be the dominant source of X-rays in models of high-z galaxies. This choice is motivated by X-ray observations of nearby star-forming galaxies (see review by Fabbiano 2006), as well as theoretical models of stellar evolution, which predict the formation of more massive stellar remnants and more binaries in metal-poor environments (e.g. Belczynski et al. 2008; Linden et al. 2010; Mapelli et al. 2010). Indeed, observations of star-forming galaxies are consistent with a boost in HMXB populations (per unit SFR) in galaxies out to $z \sim 4$–6 (Basu-Zych et al. 2013; Kaaret 2014), as is the unresolved fraction of the cosmic X-ray background (Dijkstra et al. 2012). Though direct constraints on the $z \gtrsim 4$ population are weak, local analogues of high-z galaxies exhibit a factor of $\sim$10 enhancement in the normalization of the X-ray luminosity function in metal-poor galaxies relative to galaxies with $\sim$ solar metallicity (e.g. Kaaret, Schmitt & Gorski 2011; Prestwich et al. 2013; Brorby, Kaaret & Prestwich 2014).

Even if HMXBs are the dominant sources of X-rays in the early Universe, there are various remaining uncertainties that may affect the global 21-cm signal and inferences drawn from the position of its minimum. Our focus is on modifications of the 21-cm signal brought about by variation in the characteristic mass of accreting objects and the reprocessing of their intrinsic emission spectrum by intervening material. Theoretical investigations of this sort can provide vital information to upcoming 21-cm experiments that seek to detect the absorption trough, such as the *Dark Ages Radio Explorer* (*DARE*; Burns et al. 2012), the Large Aperature Experiment to Detect the Dark Ages (LEDA; Greenhill & Bernardi 2012), and the SCI-HI experiment (Voytek et al. 2014). For instance, how accurately must the 21-cm absorption trough be measured in order to distinguish models for the first X-ray sources?

The challenge for such studies is solving the cosmological radiative transfer equation (RTE) in a way that (1) accurately couples the radiation field from sources to the thermal and ionization state of the IGM, and (2) does so quickly enough that a large volume of parameter space may be surveyed. Recent studies have taken the first steps towards this goal by identifying SEDs likely to be representative of high-z sources (e.g. Power et al. 2013). Some have applied semi-numeric schemes to predict how these SEDs contribute to the ionizing background (Fragos et al. 2013; Power et al. 2013), while others have studied the influence of realistic X-ray SEDs on the sky-averaged 21-cm signal and the 21-cm power spectrum (Ripamonti et al. 2008; Fialkov, Barkana & Visbal 2014). Our focus is complementary: rather than calculating the ionizing background strength or 21-cm signal that arise using 'best guess' inputs for the SED of X-ray sources, we quantify how reasonable deviations from best guess SEDs can complicate inferences drawn from the signal.

The outline of this paper is as follows. In Section 2, we introduce our framework for cosmological radiative transfer and the global 21-cm signal. In Section 3, we describe our implementation of the Haardt & Madau (1996) method for discretizing the RTE and test its capabilities. In Section 4, we use this scheme to investigate the impact of SED variations on the global 21-cm signal. Discussion and conclusions are in Sections 5 and 6, respectively. We adopt WMAP7+BAO+SNIa cosmological parameters ($\Omega_{\Lambda,0} = 0.728$, $\Omega_{\rm b}, 0 = 0.044$, $H_0 = 70.2$ km s^{-1} Mpc^{-1}, $\sigma_8 = 0.807$, $n = 0.96$) throughout (Komatsu et al. 2011).

2 THEORETICAL FRAMEWORK

As in Furlanetto (2006), we divide the IGM into two components: (1) the 'bulk IGM', which is mostly neutral and thus capable of producing a 21-cm signature, and (2) H II regions, which are fully ionized and thus dark at redshifted 21-cm wavelengths. This approach is expected to break down in the late stages of reionization when the distinction between H II regions and the 'neutral' IGM becomes less clear. However, our focus in this paper is on the pre-reionization era so we expect this formalism to be reasonably accurate.

There are three key steps one must take in order to generate a synthetic global 21-cm signal within this framework. Starting from a model for the volume-averaged emissivity of astrophysical sources, which we denote as $\epsilon_\nu(z)$ or $\hat{\epsilon}_\nu(z)$, further subdivided into a bolometric luminosity density (as a function of redshift) and SED (could also evolve with redshift in general), one must

(i) determine the mean radiation background pervading the space between galaxies (the so-called metagalactic radiation background), including the effects of geometrical dilution, redshifting, and bound-free absorption by neutral gas in the IGM. We denote this angle-averaged background radiation intensity as J_ν or $\widehat{J}_\nu$.

(ii) once the background intensity is in hand, compute the ionization rate density, $\Gamma_{\rm HI}$, and heating rate density, $\epsilon_{\rm X}$, in the bulk IGM.

(iii) given the ionization and heating rate densities, we can then solve for the rate of change in the ionized fraction, x_e, and temperature, T_K, of the bulk IGM gas. The rate of change in the volume filling fraction of H II regions, x_i, is related more simply to the rate of baryonic collapse in haloes above a fixed virial temperature, $T_{\rm min}$, at the redshift of interest.

Once the thermal and ionization state of the IGM and the background intensity at the Ly α resonance are known, a 21-cm signal can be computed. In this section, we will go through each of these steps in turn.

2.1 Astrophysical models

We assume throughout that the volume-averaged emissivity is proportional to the rate of collapse, $\hat{\epsilon}_\nu(z) \propto \mathrm{d}f_{\mathrm{coll}}/\mathrm{d}t$, where

$$f_{\mathrm{coll}} = \rho_{\mathrm{m}}^{-1}(z) \int_{m_{\min}}^{\infty} m n(m) \mathrm{d}m \tag{1}$$

is the fraction of gas in collapsed haloes more massive than $m_{\min}$. Here, $\rho_{\mathrm{m}}(z)$ is the mean comoving mass density of the Universe and $n(m)dm$ is the comoving number density of haloes with masses in the range $(m, m + dm)$. We compute $n(m)$ using the HMF-CALC code (Murray, Power & Robotham 2013), which depends on the Code for Anisotropies in the Microwave Background (CAMB; Lewis, Challinor & Lasenby 2000). We choose a fixed minimum virial temperature $T_{\min} \geq 10^4$ K corresponding to the atomic cooling threshold (equation 26; Barkana & Loeb 2001), which imposes redshift evolution in $m_{\min}$.

Our model for the emissivity is then

$$\epsilon_\nu(z) = \bar{\rho}_{\mathrm{b}}^0 c_i f_i \frac{\mathrm{d}f_{\mathrm{coll}}}{\mathrm{d}t} I_\nu, \tag{2}$$

where $\bar{\rho}_{\mathrm{b}}^0$ is the mean baryon density today, c_i is a physically (or observationally) motivated normalization factor that converts baryonic collapse into energy output in some emission band i (e.g. Lyα, soft UV, X-ray), while f_i is a free parameter introduced to signify uncertainty in how c_i evolves with redshift. The parameter I_ν represents the SED of astrophysical sources, and is normalized such that $\int I_\nu \mathrm{d}\nu = 1$. We postpone a more detailed discussion of our choices for c_i, I_ν, and what we mean by 'astrophysical sources' to Section 4.

2.2 Cosmological radiative transfer

Given the volume-averaged emissivity, ϵ_ν, the next step in computing the global 21-cm signal is to obtain the angle-averaged background intensity, J_ν. To do so, one must solve the cosmological RTE,

$$\left(\frac{\partial}{\partial t} - \nu H(z) \frac{\partial}{\partial \nu}\right) J_\nu(z) + 3H(z) J_\nu(z) = -c\alpha_\nu J_\nu(z) + \frac{c}{4\pi} \epsilon_\nu(z)(1+z)^3, \tag{3}$$

where H is the Hubble parameter, which we take to be $H(z) \approx H_0 \Omega_{\mathrm{m},0}(1+z)^{3/2}$ as is appropriate in the high-z matter-dominated Universe, and c is the speed of light. This equation treats the IGM as an isotropic source and sink of radiation, parametrized by the comoving volume emissivity, ϵ_ν (here in units of erg s^{-1} Hz^{-1} cMpc^{-3}, where 'cMpc' is short for 'comoving Mpc'), and the absorption coefficient, α_ν, which is related to the optical depth via $\mathrm{d}\tau_\nu = \alpha_\nu \mathrm{d}s$, where $\mathrm{d}s$ is a path length. The solution is cleanly expressed if we write the flux and emissivity in units of photon number (which we denote with 'hats', i.e. $[\widehat{J}_\nu] = $ s^{-1} cm^{-2} Hz^{-1} sr^{-1} and $[\hat{\epsilon}_\nu] = $ s^{-1} Hz^{-1} cMpc^{-3}),

$$\widehat{J}_\nu(z) = \frac{c}{4\pi}(1+z)^2 \int_z^{z_{\mathrm{f}}} \frac{\hat{\epsilon}_{\nu'}(z')}{H(z')} \mathrm{e}^{-\overline{\tau}_\nu} \mathrm{d}z'. \tag{4}$$

The 'first light redshift' when astrophysical sources first turn on is denoted by z_{f}, while the emission frequency, ν', of a photon emitted at redshift z' and observed at frequency ν and redshift z is

$$\nu' = \nu \left(\frac{1+z'}{1+z}\right). \tag{5}$$

The optical depth is a sum over absorbing species,

$$\overline{\tau}_\nu(z, z') = \sum_j \int_z^{z'} n_j(z'') \sigma_{j,\nu''} \frac{\mathrm{d}l}{\mathrm{d}z''} \mathrm{d}z'', \tag{6}$$

where $\mathrm{d}l/\mathrm{d}z = c/H(z)/(1+z)$ is the proper cosmological line element, and $\sigma_{j,\,\nu}$ is the bound-free absorption cross-section of species $j =$ H I, He I, He II with number density n_j. We use the fits of Verner & Ferland (1996) to compute $\sigma_{j,\,\nu}$ unless stated otherwise, assume the ionized fraction of hydrogen and singly ionized helium are equal (i.e. $x_{\mathrm{H\,II}} = x_{\mathrm{He\,II}}$), and neglect He II entirely (i.e. $x_{\mathrm{He\,III}} = 0$). We will revisit this helium approximation in Section 5.

The Lyα background intensity, which determines the strength of Wouthuysen–Field coupling (Wouthuysen 1952; Field 1958), is computed analogously via

$$\widehat{J}_\alpha(z) = \frac{c}{4\pi}(1+z)^2 \sum_{n=2}^{n_{\max}} f_{\mathrm{rec}}^{(n)} \int_z^{z_{\max}^{(n)}} \frac{\hat{\epsilon}_{\nu'}(z')}{H(z')} \mathrm{d}z', \tag{7}$$

where $f_{\mathrm{rec}}^{(n)}$ is the 'recycling fraction', that is, the fraction of photons that redshift into a Lyn resonance that ultimately cascade through the Lyα resonance (Pritchard & Furlanetto 2006). We truncate the sum over Lyn levels at $n_{\max} = 23$ as in Barkana & Loeb (2005), and neglect absorption by intergalactic H_2. The upper bound of the definite integral,

$$1 + z_{\max}^{(n)} = (1+z) \frac{\left[1 - (n+1)^{-2}\right]}{1 - n^{-2}}, \tag{8}$$

is set by the horizon of Lyn photons – a photon redshifting through the Lyn resonance at z could only have been emitted at $z' < z_{\max}^{(n)}$, since emission at slightly higher redshift would mean the photon redshifted through the Ly$(n+1)$ resonance.

Our code can be used to calculate the full 'sawtooth' modulation of the soft UV background (Haiman, Rees & Loeb 1997) though we ignore such effects in this work given that our focus is on X-ray heating. Preservation of the background spectrum in the Lyman–Werner band and at even lower photon energies is crucial for studies of feedback, but because we have made no attempt to model H_2 photodissociation or H^- photodetachment, we neglect a detailed treatment of radiative transfer at energies below $h\nu =$ 13.6 eV and instead assume a flat UV spectrum between Lyα and the Lyman-limit and 'instantaneous' emission only, such that the Lyα background at any redshift is proportional to the Lyα emissivity, $\hat{\epsilon}_\alpha$, at that redshift. Similarly, the growth of H II regions is governed by the instantaneous ionizing photon luminosity, though more general solutions would self-consistently include a soft UV background that arises during the EoR due to rest-frame X-ray emission from much higher redshifts.

2.3 Ionization and heating rates

With the background radiation intensity, J_ν, in hand, one can compute the ionization and heating this background causes in the bulk IGM. To calculate the ionization rate density, we integrate the background intensity over frequency,

$$\Gamma_{\mathrm{H\,I}}(z) = 4\pi n_{\mathrm{H}}(z) \int_{\nu_{\min}}^{\nu_{\max}} \widehat{J}_\nu \sigma_{\nu,\mathrm{H\,I}} \mathrm{d}\nu, \tag{9}$$

where $n_{\mathrm{H}} = \bar{n}_{\mathrm{H}}^0(1+z)^3$ and $\bar{n}_{\mathrm{H}}^0$ is the number density of hydrogen atoms today. The ionization rate in the bulk IGM due to fast secondary electrons (e.g. Shull & van Steenberg 1985; Furlanetto & Stoever 2010) is computed similarly,

$$\gamma_{\rm HI}(z) = 4\pi \sum_j n_j \int_{\nu_{\rm min}}^{\nu_{\rm max}} f_{\rm ion} \widehat{J}_\nu \sigma_{\nu,j} (h\nu - h\nu_j) \frac{{\rm d}\nu}{h\nu}, \quad (10)$$

and analogously, the heating rate density,

$$\epsilon_{\rm X}(z) = 4\pi \sum_j n_j \int_{\nu_{\rm min}}^{\nu_{\rm max}} f_{\rm heat} \widehat{J}_\nu \sigma_{\nu,j} (h\nu - h\nu_j) {\rm d}\nu, \quad (11)$$

where $h\nu_j$ is the ionization threshold energy for species j, with number density n_j, and $\nu_{\rm min}$ and $\nu_{\rm max}$ are the minimum and maximum frequency at which sources emit, respectively. $f_{\rm ion}$ and $f_{\rm heat}$ are the fractions of photoelectron energy deposited as further hydrogen ionization and heat, respectively, which we compute using the tables of Furlanetto & Stoever (2010) unless otherwise stated.

2.4 Global 21-cm signal

Finally, given the ionization and heating rates, $\Gamma_{\rm HI}$, $\gamma_{\rm HI}$, and $\epsilon_{\rm X}$, we evolve the ionized fraction in the bulk IGM via

$$\frac{{\rm d}x_{\rm e}}{{\rm d}t} = (\Gamma_{\rm HI} + \gamma_{\rm HI})(1 - x_{\rm e}) - \alpha_{\rm B} n_{\rm e} x_{\rm e} \quad (12)$$

and the volume filling factor of H II regions, x_i, via

$$\frac{{\rm d}x_i}{{\rm d}t} = f_* f_{\rm esc} N_{\rm ion} \bar{n}_{\rm b}^0 \frac{{\rm d}f_{\rm coll}}{{\rm d}t}(1 - x_{\rm e}) - \alpha_{\rm A} C(z) n_{\rm e} x_i \quad (13)$$

where $\bar{n}_{\rm b}^0$ is the baryon number density today, $\alpha_{\rm A}$ and $\alpha_{\rm B}$ are the case-A and case-B recombination coefficients, respectively, $n_{\rm e} = n_{\rm H\,II} + n_{\rm He\,II}$ is the proper number density of electrons, f_* is the star-formation efficiency, $f_{\rm esc}$ the fraction of ionizing photons that escape their host galaxies, $N_{\rm ion}$ the number of ionizing photons emitted per baryon in star formation, and $C(z)$ is the clumping factor. We average the ionization state of the bulk IGM and the volume filling factor of H II regions to determine the mean ionized fraction, i.e. $\overline{x}_i = x_i + (1 - x_i)x_{\rm e}$, which dictates the IGM optical depth (equation 6). We take $C(z)$ = constant = 1 for simplicity, as our focus is on the IGM thermal history, though our results are relatively insensitive to this choice as we terminate our calculations once the 21-cm signal reaches its emission peak, at which time the IGM is typically only ~10–20 per cent ionized.

The kinetic temperature of the bulk IGM is evolved via

$$\frac{3}{2}\frac{{\rm d}}{{\rm d}t}\left(\frac{k_{\rm B} T_k n_{\rm tot}}{\mu}\right) = \epsilon_{\rm X} + \epsilon_{\rm comp} - \mathcal{C}, \quad (14)$$

where $\epsilon_{\rm comp}$ is Compton heating rate density and $\mathcal{C}$ represents all cooling processes, which we take to include Hubble cooling, collisional ionization cooling, recombination cooling, and collisional excitation cooling using the formulae provided by Fukugita & Kawasaki (1994). Equations (12)–(14) are solved using the radiative transfer code[1] described in Mirocha et al. (2012).

Given T_K, x_i, $x_{\rm e}$, and $\widehat{J}_\alpha$, we can compute the sky-averaged 21-cm signal via (e.g. Furlanetto 2006)

$$\delta T_{\rm b} \simeq 27(1 - \overline{x}_i)\left(\frac{\Omega_{\rm b,0}h^2}{0.023}\right)\left(\frac{0.15}{\Omega_{\rm m,0}h^2}\frac{1+z}{10}\right)^{1/2}\left(1 - \frac{T_\gamma}{T_{\rm S}}\right), \quad (15)$$

where

$$T_{\rm S}^{-1} \approx \frac{T_\gamma^{-1} + x_c T_K^{-1} + x_\alpha T_\alpha^{-1}}{1 + x_c + x_\alpha} \quad (16)$$

is the excitation or 'spin' temperature of neutral hydrogen, which characterizes the number of hydrogen atoms in the hyperfine triplet state relative to the singlet state, and $T_\alpha \simeq T_K$. We compute the collisional coupling coefficient using the tabulated values in Zygelman (2005), and take $x_\alpha = 1.81 \times 10^{11} \widehat{J}_\alpha/(1+z)$, i.e. we ignore detailed line profile effects (Chen & Miralda-Escudé 2004; Chuzhoy, Alvarez & Shapiro 2006; Furlanetto & Pritchard 2006; Hirata 2006).

3 THE CODE

The first step in our procedure for computing the global 21-cm signal – determining the background radiation intensity – is the most difficult. This step is often treated approximately, by truncating the integration limits in equations 4 (for J_ν) and 11 (for $\epsilon_{\rm X}$) (e.g. Mesinger, Furlanetto & Cen 2011), or neglected entirely (e.g. Furlanetto 2006) in the interest of speed. In what follows, we will show that doing so can lead to large errors in the global 21-cm signal, but more importantly, such approaches preclude detailed studies of SED effects.

Other recent works guide the reader through equations (4) and (11), but give few details about how the equations are solved numerically (e.g. Pritchard & Furlanetto 2007; Santos et al. 2010; Tanaka et al. 2012). Brute-force solutions to equation (11) are accurate but extremely expensive, while seemingly innocuous discretization schemes introduced for speed can induce errors in the global 21-cm comparable in magnitude to several physical effects we consider in Section 4. The goal of this section is to forestall confusion about our methods, and to examine the computational expense of solving equation (11) accurately.

3.1 Discretizing the RTE

Obtaining precise solutions to equation (4) are difficult because the integrand is expensive to calculate, mostly due to the optical depth term, which is itself an integral function (equation 6). One approach that limits the number of times the integrand in equation (4) must be evaluated is to discretize in redshift and frequency, and tabulate the optical depth a priori. Care must be taken, however, as undersampling the optical depth can lead to large errors in the background radiation intensity. This technique also requires one to assume an ionization history a priori, $\overline{x}_i(z)$, which we take to be $\overline{x}_i(z)$ = constant = 0 over the redshift interval $10 \leq z \leq 40$. We defer a detailed discussion of this assumption to Section 5.

The consequences of undersampling the optical depth are shown in Fig. 1, which shows the X-ray background spectrum at $z = 20$ for a population of 10 $M_\odot$ BHs with multicolour disc (MCD) spectra (Mitsuda et al. 1984) and our default set of parameters, which will be described in more detail in Section 4 (summarized in Table 1). Soft X-rays are absorbed over small redshift intervals – in some cases over intervals smaller than those sampled in the optical depth table – which lead to overestimates of the soft X-ray background intensity. Overestimating the soft X-ray background intensity can lead to significant errors in the resulting heating since soft X-rays are most readily absorbed by the IGM (recall $\sigma_\nu \propto \nu^{-3}$ approximately). For a redshift grid with points linearly spaced by an amount Δz = {0.4, 0.2, 0.1, 0.05}, the errors in J_ν as shown in Fig. 1 correspond to relative errors in the heating rate density, $\epsilon_{\rm X}$, of {1.1, 0.44, 0.15,

[1] https://bitbucket.org/mirochaj/rt1d

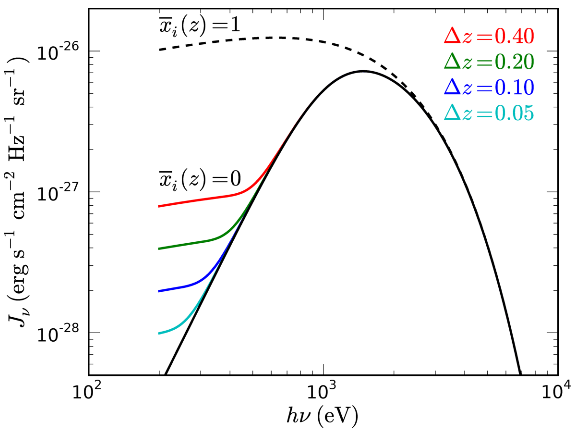

Figure 1. X-ray background intensity, J_ν, at $z = 20$ assuming a population of 10 $M_\odot$ BHs. The IGM optical depth, $\overline{\tau}_\nu$, is sampled at 128 logarithmically spaced frequencies between 0.2 and 30 keV, and linearly in redshift by $\Delta z = 0.4$ (red), 0.2 (green), 0.1 (blue), and 0.05 (cyan). Poor redshift resolution always leads to overestimates of the background intensity at soft X-ray energies ($h\nu \lesssim 0.5$ keV) since the integrand is a rapidly evolving function of redshift. The solid black line is the full numerical solution obtained by integrating equation (4) with a Gaussian quadrature technique, and the dashed black line is the same calculation assuming the optically thin $\overline{x}_i(z) = \text{constant} = 1$ limit as opposed to $\overline{x}_i(z) = \text{constant} = 0$. In order to prevent errors in J_ν at all energies $h\nu \geq 0.2$ keV, the redshift dimensions of $\overline{\tau}_\nu$ must be sampled at better than $\Delta z = 0.05$ resolution.

0.04}. Errors in ϵ_X due to frequency sampling (128 used points here) are negligible (relative error $<10^{-4}$).

To prevent the errors in ϵ_X associated with under sampling $\overline{\tau}_\nu$, we must understand how far X-rays of various energies travel before being absorbed. We estimate a characteristic differential redshift element over which photons are absorbed by assuming a fully neutral medium, and approximate bound-free photoionization cross-sections ($\sigma \propto \nu^{-3}$), in which case the optical depth (equation 6) can be written analytically as

$$\overline{\tau}_\nu(z, z') \simeq \left(\frac{\mu}{\nu}\right)^3 (1+z)^{3/2} \left[1 - \left(\frac{1+z}{1+z'}\right)^{3/2}\right], \quad (17)$$

where

$$\mu^3 \equiv \frac{2}{3} \frac{\bar{n}_{\mathrm{H}}^0 \sigma_0 c}{H_0 \sqrt{\Omega_{\mathrm{m},0}}} \left(\nu_{\mathrm{H\,I}}^3 + y \nu_{\mathrm{He\,I}}^3\right). \quad (18)$$

Here, σ_0 is the cross-section at the hydrogen ionization threshold, $h\nu_{\mathrm{H\,I}}$ and $h\nu_{\mathrm{He\,I}}$ are the ionization threshold energies for hydrogen and helium, respectively, y is the primordial helium abundance by number, H_0 the Hubble parameter today, and $\Omega_{\mathrm{m},0}$ the matter density relative to the critical density today.

The characteristic energy $h\mu \simeq 366.5$ eV may be more familiar as it relates to the mean-free paths of photons in a uniform medium relative to the Hubble length, which we refer to as 'Hubble photons', with energy $h\nu_{\mathrm{Hub}}$,

$$\begin{aligned} h\nu_{\mathrm{Hub}} &\simeq h\mu \left[\tfrac{3}{2}\right]^{1/3} (1-x_i)^{1/3} (1+z)^{1/2} \\ &\simeq 1.5 (1-x_i)^{1/3} \left(\tfrac{1+z}{10}\right)^{1/2} \ \mathrm{keV}. \end{aligned} \quad (19)$$

The characteristic differential redshift element of interest (which we refer to as the 'bound-free horizon' and denote Δz_{bf}) can be derived by setting $\tau_\nu(z, z') = 1$ and taking $z' = z + \Delta z_{\mathrm{bf}}$ in equation (17). The result is

$$\Delta z_{\mathrm{bf}} \simeq (1+z) \left\{ \left[1 - \left(\frac{\nu/\mu}{\sqrt{1+z}}\right)^3\right]^{-2/3} - 1 \right\}. \quad (20)$$

That is, a photon with energy $h\nu$ observed at redshift z has experienced an optical depth of 1 since its emission at redshift $z + \Delta z_{\mathrm{bf}}$ and energy $h\nu[1 + \Delta z_{\mathrm{bf}}/(1+z)]$. Over the interval $10 \lesssim z \lesssim 40$, this works out to be $0.1 \lesssim \Delta z_{\mathrm{bf}} \lesssim 0.2$ assuming a photon with frequency $\nu = \mu$.

In order to accurately compute the flux (and thus heating), one must resolve this interval with at least a few points, which explains the convergence in Fig. 1 once $\Delta z \leq 0.1$ for $h\nu \lesssim 350$ eV. We discretize logarithmically in redshift (for reasons that will become clear momentarily) following the procedure outlined in appendix C of Haardt & Madau (1996), first defining

$$x \equiv 1 + z, \quad (21)$$

which allows us to set up a logarithmic grid in x-space such that

$$R \equiv \frac{x_{l+1}}{x_l} = \text{constant}, \quad (22)$$

where $l = 0, 1, 2, \ldots, n_z - 1$. The corresponding grid in photon energy space is

$$h\nu_n = h\nu_{\min} R^{n-1}, \quad (23)$$

where $h\nu_{\min}$ is the minimum photon energy we consider, and $n = 1, 2, \ldots, n_\nu$. The number of frequency bins, n_ν, can be determined iteratively in order to guarantee coverage out to some maximum emission energy, $h\nu_{\max}$.

The emission frequency, $\nu_{n'}$, of a photon observed at frequency $h\nu_n$ and redshift z_l, emitted at redshift z_m is then (i.e. a discretized form of equation 5)

$$\nu_{n'} = \nu_n \left(\frac{1+z_m}{1+z_l}\right), \quad (24)$$

meaning $\nu_{n'}$ can be found in our frequency grid at index $n' = n + m - l$.

The advantage of this approach still may not be immediately obvious, but consider breaking the integral of equation (4) into two pieces, an integral from z_l to z_{l+1}, and an integral from z_{l+1} to z_{n_z-1}. In this case, equation (4) simplifies to

$$\begin{aligned} \widehat{J}_{\nu_n}(z_l) &= \frac{c}{4\pi}(1+z_l)^2 \int_{z_l}^{z_{l+1}} \frac{\hat{\epsilon}_{\nu_{n'}}(z')}{H(z')} \mathrm{e}^{-\overline{\tau}_{\nu_n}(z_l, z')} \mathrm{d}z' \\ &+ \left(\frac{1+z_l}{1+z_{l+1}}\right)^2 \widehat{J}_{\nu_{n+1}}(z_{l+1}) \mathrm{e}^{-\overline{\tau}_{\nu_n}(z_l, z_{l+1})}. \end{aligned} \quad (25)$$

The first term accounts for 'new' flux due to the integrated emission of sources at $z_l \leq z \leq z_{l+1}$, while the second term is the flux due to emission from all $z > z_{l+1}$, i.e. the background intensity at z_{l+1} corrected for geometrical dilution and attenuation between z_l and z_{l+1}.

Equation (25) tells us that by discretizing logarithmically in redshift and iterating from high redshift to low redshift we can keep a 'running total' on the background intensity. In fact, we must never explicitly consider the case of $m \neq l + 1$, meaning equation (24) is simply $\nu_{n'} = R\nu_n = \nu_{n+1}$. The computational cost of this algorithm is independent of redshift, since the flux at z_l only ever depends on quantities at z_l and z_{l+1}. Such is not the case for a brute-force integration of equation (4), in which case the redshift interval increases with time. The logarithmic approach also limits memory

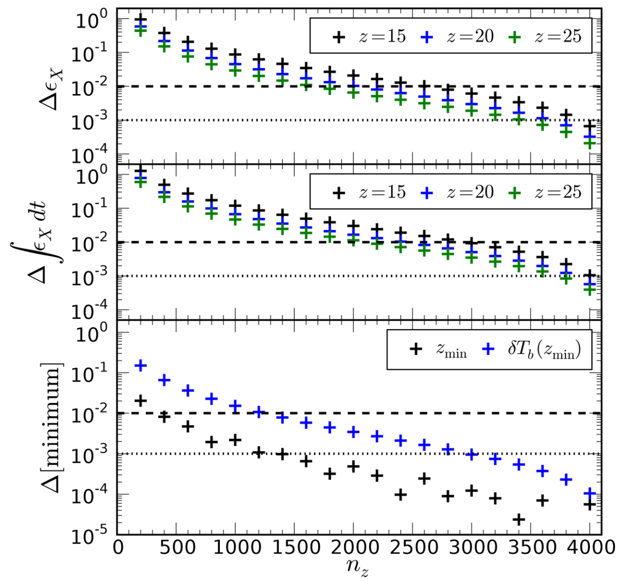

Figure 2. Accuracy of presented algorithm. Top: relative error in the heating rate density, $\epsilon_{\rm X}$, as a function of the number of redshift points, n_z, used to sample $\overline{\tau}_\nu$, as compared to a brute-force solution to equation (11) using a double Gaussian quadrature integration scheme. Middle: relative error in the cumulative heating as a function of n_z. Bottom: relative error in the position of the 21-cm minimum, in redshift (black crosses) and amplitude (blue crosses). Dotted and dashed lines indicate 0.1 per cent and 1 per cent errors, respectively.

consumption, since we need not tabulate the flux or optical depth in 3D – we only ever need to know the optical depth between redshifts z_l and z_{l+1} – in addition to the fact that we can discard the flux at z_{l+2}, $J_\nu(z_{l+2})$, once we reach z_l. A linear discretization scheme would require 3D optical depth tables with $n_\nu n_z^2$ elements, which translates to tens of gigabytes of memory for the requisite redshift resolution (to be discussed in the next subsection).

Finally, linear discretization schemes prevent one from keeping a 'running total' on the background intensity, since the observed flux at redshift z_l and frequency ν_n cannot (in general) be traced back to rest frame emission from redshifts $z_{l'}$ or frequencies $\nu_{n'}$ within the original redshift and frequency grids (over l and n). The computational cost of performing the integral in equation (4) over all redshifts $z' > z$ is prohibitive, as noted by previous authors (e.g. Mesinger et al. 2011).

3.2 Accuracy and expense

The accuracy of this approach is shown in Fig. 2 as a function of the number of redshift bins in the optical depth lookup table, n_z. Errors in the heating rate density (top), and cumulative heating (middle), $\Delta \int \epsilon_{\rm X} {\rm d}t$, drop below 0.1 per cent at all $10 \le z \le 40$ once $n_z \gtrsim 4000$, at which time errors in the position of the 21-cm minimum (bottom) are accurate to $\sim$0.01 per cent. Given this result, all calculations reported in Section 4 take $n_z = 4000$. For reference, errors of the order of 0.1 per cent correspond to $\sim$0.1 mK errors in the amplitude of the 21-cm minimum in our reference model, which we will soon find is much smaller than the changes induced by physical effects.

Many previous studies avoided the expense of equation (4) by assuming that a constant fraction of the X-ray luminosity density is deposited in the IGM as heat (e.g. Furlanetto 2006). A physically motivated approximation is to assume that photons with short mean-free paths (e.g. those that experience $\overline{\tau}_\nu \le 1$) are absorbed and contribute to heating, and all others do not (e.g. Mesinger et al. 2011). This sort of 'step attenuation' model was recently found to hold fairly well in the context of a fluctuating X-ray background, albeit for a single set of model parameters (Mesinger & Furlanetto 2009).

An analogous estimate for the heating caused by a uniform radiation background assumes that photons with mean-free paths shorter than a Hubble length are absorbed, and all others are not. We define $\xi_{\rm X}$ as the fraction of the bolometric luminosity density that is absorbed locally, which is given by

$$\xi_{\rm X}(z) \approx \int_{\nu_{\rm min}}^{\nu_{\rm Hub}} I_\nu {\rm d}\nu \left(\int_{\nu_{\rm min}}^{\nu_{\rm max}} I_\nu {\rm d}\nu \right)^{-1}, \tag{26}$$

where $h\nu_{\rm Hub}$ is given by equation (19). There are approximate analytic solutions to the above equation for power-law sources (would be exact if not for the upper integration limit, $\nu_{\rm Hub}$), though $\xi_{\rm X}$ must be computed numerically for the MCD spectra we consider. We take $h\nu_{\rm min} = 200$ eV and $h\nu_{\rm max} = 30$ keV for the duration of this paper. The heating rate density associated with a population of objects described by $\xi_{\rm X}$ and $\mathcal{L}_{\rm bol}$ is

$$\epsilon_{\rm X}(z) = \xi_{\rm X}(z) \mathcal{L}_{\rm bol}(z) f_{\rm heat}, \tag{27}$$

where $f_{\rm heat}$ is the fraction of the absorbed energy that is deposited as heat. Because there is no explicit dependence on photon energy in this approximation, we use the fitting formulae of Shull & van Steenberg (1985) to compute $f_{\rm heat}$.

The consequences of using equations (26) and (27) for the global 21-cm signal are illustrated in Fig. 3. Steep power-law sources can be modelled quite well (signal accurate to 1–2 mK) using equations (26) and (27) since a large fraction of the X-ray emission occurs at low energies. In contrast, heating by sources with increasingly flat (decreasing spectral index α) spectra is poorly modelled by equations (26) and (27), inducing errors in the global 21-cm signal of order $\sim$5 mK ($\alpha = -1.5$) and $\sim$15 mK ($\alpha = -0.5$). The same trend holds for heating dominated by sources with an MCD spectrum, in which case harder spectra correspond to less massive BHs. We will see in the next section that these errors are comparable to the differences brought about by real changes in the SED of X-ray sources.

4 ACCRETING BHs IN THE EARLY UNIVERSE

Using the algorithm presented in the previous section, we now investigate the effects of varying four parameters that govern the SED of an accreting BH: (1) the mass of the BH, $M_\bullet$, which determines the characteristic temperature of an optically thick geometrically thin disc (Shakura & Sunyaev 1973), (2) the fraction of disc photons that are up-scattered (Shapiro, Lightman & Eardley 1976) by a hot electron corona, $f_{\rm sc}$, (3) the power-law index[2] of the resulting emission, α (using the SIMPL model; Steiner et al. 2009), and (4) the column density of neutral hydrogen that lies between the accreting system and the IGM, $N_{\rm HI}$. Because we assume $x_{\rm H\,II} = x_{\rm He\,II}$, the absorbing column density actually has an optical depth of $\tau_\nu = N_{\rm HI}\sigma_{\nu,{\rm H\,I}}(1 + y\sigma_{\nu,{\rm He\,I}}/\sigma_{\nu,{\rm H\,I}})$, where y is the primordial helium abundance by number, and σ_ν is the bound-free absorption cross-section for H I and He I. A subset of the spectral

[2] We define the spectral index as $L_\nu \propto \nu^\alpha$, where L_ν is a specific luminosity proportional to the *energy* of a photon with frequency ν, per logarithmic frequency interval dν.

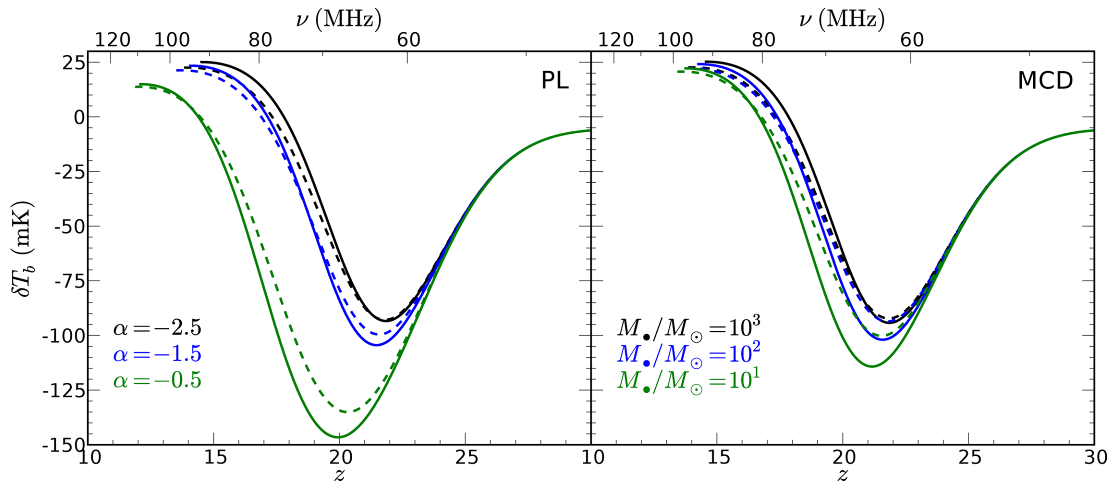

Figure 3. Testing the approximation of equations (26) and (27). Dashed lines represent the approximate solutions, while solid lines represent the full solution for the global 21-cm signal using the procedure outlined in Section 3. Left: X-ray sources are assumed to have power-law (PL) SEDs with spectral index α, extending from 0.2 to 30 keV. Right: X-ray sources are assumed to have MCD SEDs (Mitsuda et al. 1984). All sources have been normalized to have the same luminosity density above 0.2 keV (3.4×10^{40}erg s^{-1} (M$_\odot$ yr^{-1})$^{-1}$), and all calculations are terminated once the emission peak ($12 \lesssim z \lesssim 14$) has been reached. For the hardest sources of X-rays considered (left: $\alpha = -0.5$, right: $M_\bullet = 10$ M$_\odot$), the global 21-cm minimum is in error by up to $\sim$15 mK in amplitude and $\Delta z \simeq 0.5$ in position when equation (26) is used to compute $\epsilon_{\rm X}$.

models we consider is shown in Fig. 4. Note that more efficient Comptonization (i.e. increasing $f_{\rm sc}$) and strong neutral absorption (increased $N_{\rm HI}$) act to harden the intrinsic disc spectrum (top panel), while increasing the characteristic mass of accreting BHs acts to soften the spectrum (bottom panel).

To compute the X-ray heating as a function of redshift, $\epsilon_{\rm X}(z)$, we scale our SED of choice to a comoving (bolometric) luminosity density assuming that a constant fraction of gas collapsing on to haloes accretes on to BHs, i.e.

$$\dot{\rho}_\bullet(z) = f_\bullet \bar{\rho}_{\rm b}^0 \frac{{\rm d}f_{\rm coll}(T_{\rm min})}{{\rm d}t}. \tag{28}$$

Assuming Eddington-limited accretion, we obtain a comoving bolometric ‘accretion luminosity density’,

$$\mathcal{L}_{\rm acc} = 6.3 \times 10^{40}\ {\rm erg\ s^{-1}\ cMpc^{-3}} \times \left(\frac{0.9}{\xi_{\rm acc}}\right)\left(\frac{\dot{\rho}_\bullet(z)}{10^{-6}\ {\rm M_\odot\ yr^{-1}\ cMpc^{-3}}}\right), \tag{29}$$

where

$$\xi_{\rm acc} = \frac{1-\eta}{\eta} f_{\rm edd} \tag{30}$$

and η and $f_{\rm edd}$ are the radiative efficiency and Eddington ratio, respectively. To be precise, $f_{\rm edd}$ represents the product of the Eddington ratio and duty cycle, i.e. what fraction of the time X-ray sources are actively accreting, which are completely degenerate. This parametrization is very similar to that of Mirabel et al. (2011), though we do not explicitly treat the binary fraction, and our expression refers to the bolometric luminosity density rather than the 2–10 keV luminosity density. Our model for the comoving X-ray emissivity is then

$$\hat{\epsilon}_\nu(z) = \mathcal{L}_{\rm acc}(z)\frac{I_\nu}{h\nu}, \tag{31}$$

where I_ν once again represents the SED of X-ray sources, and is normalized such that $\int_0^\infty I_\nu {\rm d}\nu = 1$. Power-law sources must truncate the integration limits in this normalization integral so as to avoid divergence at low energies, though MCD models do not, since the soft X-ray portion of the spectrum is limited by the finite size of the accretion disc (which we take to be $r_{\rm max} = 10^3\, R_g$, where $R_g = GM_\bullet/c^2$).

It is common in the 21-cm literature to instead relate the comoving X-ray luminosity density, $L_{\rm X}$, to the SFR density, $\dot{\rho}_*$, as

$$L_{\rm X} = c_{\rm X} f_{\rm X} \dot{\rho}_*(z), \tag{32}$$

where the normalization factor $c_{\rm X}$ is constrained by observations of nearby star-forming galaxies (e.g. Grimm, Gilfanov & Sunyaev 2003; Ranalli, Comastri & Setti 2003; Gilfanov, Grimm & Sunyaev 2004), and $f_{\rm X}$ parametrizes our uncertainty in how the $L_{\rm X}$–SFR relation evolves with redshift. The detection of a 21-cm signal consistent with $f_{\rm X} > 1$ could provide indirect evidence of a top-heavy stellar initial mass function (IMF) at high-z since $f_{\rm X}$ encodes information about the abundance of high-mass stars and the binary fraction, both of which are expected to increase with decreasing metallicity.

However, assumptions about the SED of X-ray sources are built-in to the definition of $f_{\rm X}$. The standard value of $c_{\rm X} = 3.4 \times 10^{40}$ erg s^{-1} (M$_\odot$ yr^{-1})$^{-1}$ (Furlanetto 2006) is an extrapolation of the 2–10 keV $L_{\rm X}$–SFR relation of Grimm et al. (2003), who found $L_{2-10\ {\rm keV}} = 6.7 \times 10^{39}$ erg s^{-1} (M$_\odot$ yr^{-1})$^{-1}$, to all energies $h\nu >$ 200 eV assuming an $\alpha = -1.5$ power-law spectrum. This means any inferences about the stellar IMF at high-z drawn from constraints on $f_{\rm X}$ implicitly assume an $\alpha = -1.5$ power-law spectrum at photon energies above 0.2 keV. Because our primary interest is in SED effects, we avoid the $f_{\rm X}$ parametrization and keep the normalization of the X-ray background (given by $\dot{\rho}_\bullet/\xi_{\rm acc}$) and its SED ($I_\nu$) separate. We note that if one adopts a pure MCD spectrum (i.e. $f_{\rm sc} = N_{\rm HI} = 0$) for a 10 M$_\odot$ BH and set $f_\bullet = 10^{-5}$ (as in our reference model), the normalization of equation (29) corresponds to $f_{\rm X} \approx 2 \times 10^3$ assuming $c_{\rm X} = 2.61 \times 10^{39}$ erg s^{-1} (M$_\odot$ yr)$^{-1}$ (Mineo, Gilfanov & Sunyaev 2012b). Despite this enhancement in the total X-ray luminosity density, our reference model produces an absorption trough at $z \approx 22$ and $\delta T_{\rm b} \approx -100$ mK, similar to past work that assumed $f_{\rm X} = 1$. This is a result of our choice for the reference spectrum, a MCD, which is much harder than the $\alpha = -1.5$ power-law spectrum originally used to define $f_{\rm X}$.

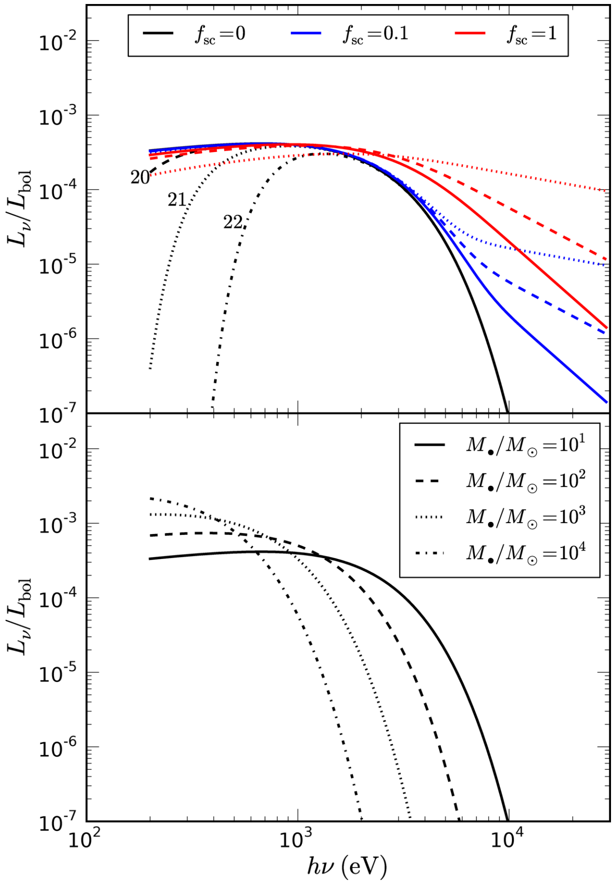

Figure 4. Subset of SEDs used in this work. Top panel: assuming $M_\bullet = 10\ M_\odot$, varying the fraction of disc photons scattered into the high-energy power-law tail, f_{sc}, and the spectral index of the resulting high-energy emission, α, using the SIMPL model (Steiner et al. 2009). Solid, dashed, and dotted lines of different colours correspond to high energy emission with power-law indices of $\alpha = -2.5$, $\alpha = -1.5$, and $\alpha = -0.5$ respectively, with the colour indicating f_{sc} as shown in the legend. Bottom panel: pure MCD SEDs for $M_\bullet = 10$–$10^4\ M_\odot$, with no intrinsic absorption or Comptonization of the disc spectrum. The solid black line is our reference model, and is the same in both panels.

Our main result is shown in Fig. 5. The effects of the coronal physics parameters f_{sc} and α are shown in the left-hand panel, and only cause deviations from the reference model if $f_{sc} > 0.1$ (for any $-2.5 \leq \alpha \leq -0.5$). Increasing f_{sc} and decreasing α act to harden the spectrum, leading to a delay in the onset of heating and thus deeper absorption feature. With a maximal value of $f_{sc} = 1$ and hardest power-law SED of $\alpha = -0.5$, the absorption trough becomes deeper by $\sim$10 mK. In the right-hand panel, we adopt $f_{sc} = 0.1$ and $\alpha = -1.5$, and turn our attention to the characteristic mass of accreting BHs and the neutral absorbing column, varying each by a factor of 100, each of which has a more substantial impact individually on the 21-cm signal than f_{sc} and α. The absorption trough varies in amplitude by up to $\sim$50 mK and in position by $\Delta z \approx 2$ from the hardest SED ($M_\bullet = 10\ M_\odot$, $N_{HI} = 10^{22}$ cm^{-2}) to softest SED ($M_\bullet = 10^3\ M_\odot$, $N_{HI} = 0$ cm^{-2}) we consider. The absorbing column only becomes important once $N_{HI} \gtrsim 10^{20}$ cm^{-2}.

Our study is by no means exhaustive. Table 1 lists parameters held constant for the calculations shown in Fig. 5. Our choices for several parameters in Table 1 that directly influence the thermal history will be discussed in the next section. While several other parameters could be important in determining the locations of 21-cm features, for instance, N_{ion} is likely $\gg$4000 for Population III (PopIII) stars (e.g. Bromm, Kudritzki & Loeb 2001; Schaerer 2002; Tumlinson, Shull & Venkatesan 2003), we defer a more complete exploration of parameter space, and assessment of degeneracies between parameters, to future work.

5 DISCUSSION

The findings of the previous section indicate that uncertainty in the SED of X-ray sources at high-z could be a significant complication in the interpretation of upcoming 21-cm measurements. Details of Comptonization are a secondary effect in this study, though still at the level of measurement errors predicted by current signal extraction algorithms (likely $\sim$10 mK for the absorption trough; Harker et al. 2012). The characteristic mass of accreting BHs, $M_\bullet$, and the amount of absorption intrinsic to BH host galaxies, parametrized by a neutral hydrogen column density N_{HI}, influence the signal even more considerably. In this section, we examine these findings in the context of other recent studies and discuss how our methods and various assumptions could further influence our results.

5.1 An evolving IGM optical depth

Central to our approach to solving equation (4) is the ability to tabulate the IGM optical depth (equation 6). This requires that we assume a model for the ionization history a priori, even though the details of the X-ray background will in general influence the ionization history to some degree.[3] Because we focus primarily on 21-cm features expected to occur at $z > 10$, we assume $\bar{x}_i = x_e = 0$ at all $z > 10$ when generating $\bar{\tau}_\nu(z, z')$.

The effects of this approximation are shown in Fig. 6, in which we examine how different ionization histories (and thus IGM opacities) affect the background flux, J_ν. Because we assume a neutral IGM for all $z \geq 10$, we always underestimate the background flux, since an evolving IGM optical depth due to reionization of the IGM allows X-rays to travel further than they would in a neutral medium. The worst-case-scenario for this $\bar{x}_i(z) = 0$ approximation occurs for very extended ionization histories (blue line in top panel of Fig. 6), in which case the heating rate density at $z = \{10, 12, 14\}$ is in error by factors of $\{1.2, 0.5, 0.2\}$. Because the 21-cm signal is likely insensitive to ϵ_X once reionization begins,[4] we suspect this error is negligible in practice. As pointed out in Mirocha et al. (2013), the 21-cm emission feature can serve as a probe of ϵ_X so long as independent constraints on the ionization history are in hand. In this case, we would simply tabulate $\bar{\tau}_\nu$ using the observational constraints on $\bar{x}_i(z)$, and mitigate the errors shown in Fig. 6. Our code could also be modified to compute the optical depth on-the-fly once $\bar{x}_i$ exceeds a few per cent, indicating the beginning of the EoR.

[3] Evolution of the volume filling factor of H II regions, x_i, is the same in each model we consider because we have not varied the number of ionizing photons emitted per baryon of star formation, N_{ion}, or the star formation history, parametrized by the minimum virial temperature of star-forming haloes, T_{min}, and the star formation efficiency, f_*. X-rays are only allowed to ionize the bulk IGM in our formalism, whose ionized fraction is $x_e \lesssim 0.1$ per cent at all $z \gtrsim 12$ in our models, meaning $\bar{x}_i \approx x_i$. The mid-point of reionization occurs at $z \simeq 10.8$ in each model we consider.

[4] Though 'cold reionization' scenarios have not been completely ruled out, recent work is inconsistent with a completely unheated $z \approx 8$ IGM (Parsons et al. 2014).

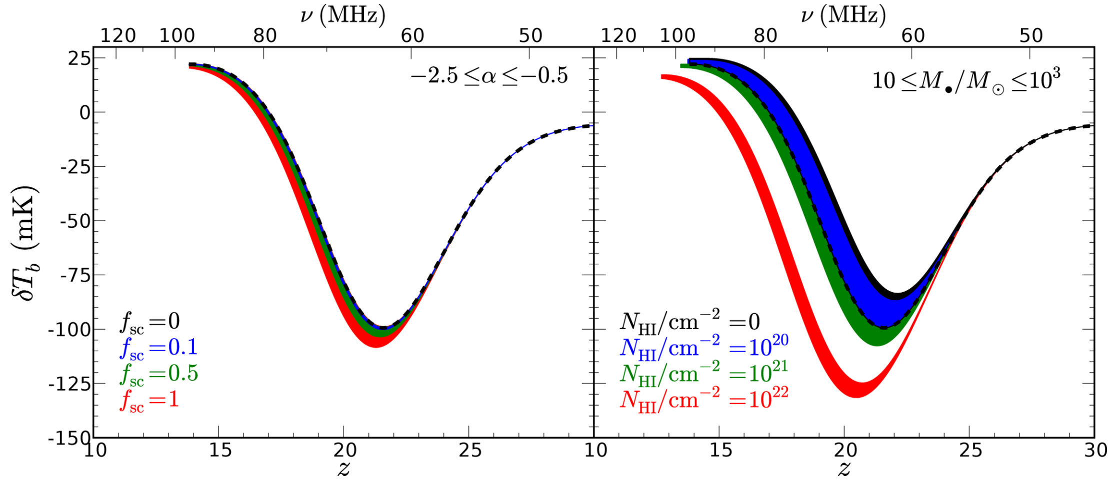

Figure 5. Evolution of the 21-cm brightness temperature for different BH SED models. Left: effects of coronal physics, parametrized by the fraction of disc photons up-scattered by a hot electron corona, f_{sc}, and the resulting spectral index of up-scattered emission, α, using the SIMPL Comptonization model of Steiner et al. (2009). The colours correspond to different values of f_{sc}, while the width of each band represents models with $-2.5 \le \alpha \le -0.5$ (the upper edge of each band corresponds to the softest SED at fixed f_{sc}, in this case $\alpha = -2.5$). Right: effects of BH mass and neutral absorbing column. Colours correspond to N_{HI}, while the width of each band represents models with $10 \le M_\bullet/\mathrm{M}_\odot \le 10^3$ (the upper edge of each band corresponds to the softest SED at fixed N_{HI}, in this case $M_\bullet = 10^3\ \mathrm{M}_\odot$). The dashed black line is our reference 'pure MCD' model with $M_\bullet = 10\ \mathrm{M}_\odot$. The black and blue regions overlap considerably, indicating that absorbing columns of $N_{HI} \gtrsim 10^{20}\ \mathrm{cm}^2$ are required to harden the spectrum enough to modify the thermal history. Every realization of the signal here has the exact same ionization history, Lyα background history, and BH accretion history. As in Fig. 3, all calculations are terminated once the peak in emission is reached. Coronal physics influences the global 21-cm minimum at the $\lesssim 10$ mK level, while $M_\bullet$ is a 10–20 mK effect and N_{HI} is potentially a ~50 mK effect.

Table 1. Parameters held constant in this work. Note that PS in the first row refers to the original analytic halo mass function derived by Press & Schechter (1974). Our reference model adopts this set of parameters and a pure MCD spectrum (i.e. $N_{HI} = f_{sc} = 0$) assuming a characteristic BH mass of $M_\bullet = 10\ \mathrm{M}_\odot$.

Parameter	Value	Description
`hmf`	PS	Halo mass function
T_{min}	10^4 K	Min. virial temperature of star-forming haloes
μ	0.61	Mean molecular weight of collapsing gas
f_*	10^{-1}	Star formation efficiency
$f_\bullet$	10^{-5}	Fraction of collapsing gas accreted on to BHs
N_{LW}	9690	Photons per stellar baryon with $\nu_\alpha \le \nu \le \nu_{LL}$
N_{ion}	4000	Ionizing photons emitted per stellar baryon
f_{esc}	0.1	Escape fraction
r_{in}	$6\,R_g$	Radius of inner edge of accretion disc
r_{max}	$10^3\,R_g$	Max. radius of accretion disc
η	0.1	Radiative efficiency of accretion
f_{edd}	0.1	Product of Eddington ratio and duty cycle
$h\nu_{min}$	0.2 keV	Softest photon considered
$h\nu_{max}$	30 keV	Hardest photon considered

5.2 Neutral absorption

Our choice of N_{HI} is consistent with the range of values adopted in the literature in recent years (e.g. Mesinger, Ferrara & Spiegel 2013), which are chosen to match constraints on neutral hydrogen absorption seen in high-z gamma-ray burst spectra (which can also be explained if reionization is patchy or not complete by $z \approx 7$; Totani et al. 2006; Greiner et al. 2009). If we assume that the absorbing column is due to the host galaxy interstellar medium (ISM), then it cannot be used solely to harden the X-ray spectrum – it must also attenuate soft UV photons from stars, and thus be related to the escape fraction of ionizing radiation, f_{esc}. In the most optimistic case of a PopIII galaxy (which we take to be a perfect blackbody of 10^5 K), an absorbing column of $N_{HI} = 10^{18.5}\ \mathrm{cm}^{-2}$ corresponds to $f_{esc} \simeq 0.01$, meaning every non-zero column density we investigated in Fig. 5 would lead to the attenuation of more than 99 per cent of ionizing stellar radiation, thus inhibiting the progression of cosmic reionization considerably.

An alternative is to assume that the absorbing column is intrinsic to accreting systems, though work on galactic X-ray binaries casts doubt on such an assumption. Miller, Cackett & Reis (2009) monitored a series of photoelectric absorption edges during BH spectral state transitions, and found that while the soft X-ray spectrum varied considerably, the column densities inferred by the absorption edges remained roughly constant. This supports the idea that evolution in the soft X-ray spectrum of X-ray binaries arises due to evolution in the source spectrum, and that neutral absorption is dominated by the host galaxy ISM.

For large values of N_{HI}, reionization could still proceed if the distribution of neutral gas in (at least some) galaxies were highly anisotropic. Recent simulations by Gnedin, Kravtsov & Chen (2008) lend credence to this idea, displaying order-of-magnitude deviations in the escape fraction depending on the propagation direction of ionizing photons – with radiation escaping through the polar regions of disc galaxies preferentially. Wise & Cen (2009) performed a rigorous study of ionizing photon escape using simulations of both idealized and cosmological haloes, reaching similar conclusions extending to lower halo masses. The higher mass haloes in the Wise & Cen (2009) simulation suite exhibited larger covering fractions of high column density gas (e.g. Fig. 10), which could act to harden the spectrum of such galaxies, in addition to causing very anisotropic H II regions.

If there existed a population of miniquasars powered by intermediate mass BHs, and more massive BHs at high-z occupy more massive haloes, then more massive haloes should have softer X-ray spectra (see Fig. 4) and thus heat the IGM more efficiently. However, if they also exhibit larger covering fractions of high column

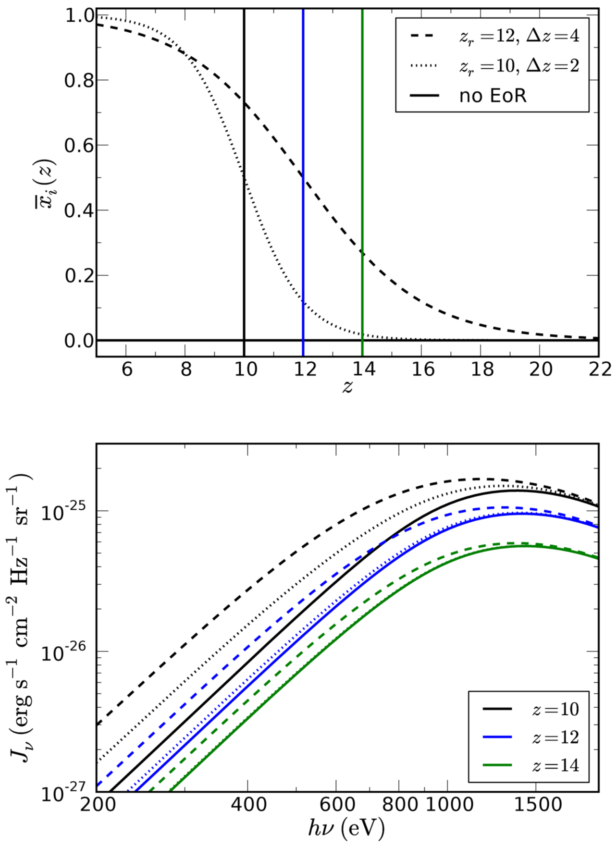

Figure 6. Consequences of the $\overline{x}_i = \text{constant} = 0$ approximation on the background radiation field for our reference model (see Table 1). Top: tanh ionization histories considered, i.e. $\overline{x}_i(z) \propto \tanh((z - z_r)/\Delta z)$. Bottom: angle-averaged background intensity, J_ν, at $z = 10$, 12 and 14 (black, blue, green) assuming a neutral IGM for all z (solid), compared to increasingly early and extended reionization scenarios (dotted and dashed). Errors in the background intensity due to the $\overline{x}_i = \text{constant} = 0$ could be important at $z \lesssim 14$, assuming early and extended reionization scenarios (e.g. $z_r = 12$, $\Delta z = 4$), though by this time the global 21-cm signal is likely insensitive to the thermal history.

density gas, the soft X-ray spectrum will be attenuated to some degree – perhaps enough to mimic an intrinsically harder source of X-rays. This effect may be reduced in galaxies hosting an AGN, since X-rays partially ionize galactic gas and thus act to enhance the escape fraction of hydrogen- and helium- ionizing radiation (Benson, Venkatesan & Shull 2013). Ultimately, the 21-cm signal only probes the volume-averaged emissivity, so if soft X-ray sources reside in high-mass haloes, they would have to be very bright to compensate for their rarity, and to contribute substantially to the heating of the IGM.

Lastly, it is worth mentioning that the hardness of the radiation field entering the 'neutral' bulk IGM is not the same as that of the radiation field leaving the galaxy (whose edge is typically defined as its virial radius) since our model treats H II regions and the bulk IGM separately. As a result, there is an extra step between the intrinsic emission (that leaving the virial radius) and the IGM: Of the photons that escape the virial radius, what fraction of them (as a function of frequency) contribute to the growth of the galactic H II region? The IGM penetrating radiation field is hardened as a result, and could become even harder and more anisotropic based on the presence or absence of large-scale structure such as dense sheets and filaments.[5] Additionally, sources with harder spectra lead to more spatially extended ionization fronts, whose outskirts could be important sources of 21-cm emission (e.g. Venkatesan & Benson 2011).

5.3 Accretion physics

We have assumed throughout a radiative efficiency of $\eta = 0.1$, which is near the expected value for a thin disc around a non-spinning BH assuming the inner edge of the disc corresponds to the innermost stable circular orbit, i.e. $r_{\text{in}} = r_{\text{isco}} = 6R_g$. The radiative efficiency is very sensitive to BH spin, varying between $0.05 \leq \eta \leq 0.4$ (Bardeen 1970) from maximal retrograde spin (disc and BH angular momentum vectors are antiparallel), to maximal prograde spin (disc and BH 'rotate' in the same sense). While the spin of stellar mass BHs is expected to be more-or-less constant after their formation (King & Kolb 1999), the spin distribution at high-z is expected to be skewed towards large values of the spin parameter, leading to enhanced radiative efficiencies $\eta > 0.1$ (Volonteri et al. 2005).

Our choice of $f_{\text{edd}} = 0.1$ is much less physically motivated, being that it is difficult both to constrain observationally and predict theoretically. For X-ray binaries, f_{edd} should in general be considered not just what fraction of time the BH is actively accreting, but what fraction of the time it is in the high/soft state when the MCD model is appropriate. We ignore this for now as it is poorly constrained, but note that the emission during the high/soft state could dominate the heating even if more time is spent in the low/hard state simply because it is soft X-rays that dominate the heating.

While we do not explicitly attempt to model nuclear BHs, equation (28) could be used to model their comoving emissivity. Note, however, that this model is not necessarily self-consistent. We have imposed an accretion history via the parameters $f_\bullet$ and $T_{\min}$, though the Eddington luminosity density depends on the mass density of BHs. For extreme models (e.g. large values of $f_\bullet$), the mass density of BHs required to sustain a given accretion luminosity density can exceed the mass density computed via integrating the accretion rate density over time. To render such scenarios self-consistent, one must require BH formation to cease or the ejection rate of BHs from galaxies to become significant (assuming ejected BHs no longer accrete), or both. The value of $f_\bullet$ we adopt is small enough that we can neglect these complications for now, and postpone more detailed studies including nuclear BHs to future work.

5.4 Choosing representative parameter values

The results of recent population synthesis studies suggest that X-ray binaries are likely to be the dominant source of X-rays at high-z. Power et al. (2013) modelled the evolution of a single stellar population that forms in an instantaneous burst, tracking massive stars

[5] In fact, the metagalactic background could be even harder than this, given that soft X-rays are absorbed on small scales and thus may not deserve to be included in a 'global' radiation background. Madau et al. (2004) argued for $E_{\min} = 150$ eV since 150 eV photons have a mean-free path comparable to the mean separation between sources in their models, which formed in 3.5σ density peaks at $z \sim 24$. However, for rare sources, a global radiation background treatment may be insufficient (e.g. Davies & Furlanetto 2014). We chose $E_{\min} = 0.2$ keV to be consistent with other recent work on the 21-cm signal (e.g. Pritchard & Loeb 2012), but clearly further study is required to determine reasonable values for this parameter. At least for large values of N_{HI}, the choice of $E_{\min}$ is irrelevant.

evolving off the main sequence, and ultimately the X-ray binaries that form. Taking Cygnus X-1 as a spectral template, they compute the ionizing luminosity of the population with time (assuming a Kroupa IMF) and find that HMXBs dominate the instantaneous ionizing photon luminosity starting 20–30 Myr after the initial burst of star formation depending on the binary survival fraction. Fragos et al. (2013) performed a similar study, but instead started from the Millennium II simulation halo catalogue and applied population synthesis models to obtain the evolution of the background X-ray spectrum and normalization from $z \sim 20$ to present day. They find that X-ray binaries could potentially dominate the X-ray background over AGN (at least from 2 to 10 keV) at all redshifts higher than $z \sim 5$.

Though our reference model effectively assumes that HMXBs dominate the X-ray background at high-z, supernovae (Oh 2001; Furlanetto & Loeb 2004), accreting intermediate-mass BHs, whether they be solitary 'miniquasars' (e.g. Haiman & Loeb 1998; Wyithe & Loeb 2003; Kuhlen & Madau 2005) or members of binaries, and thermal bremsstrahlung radiation from the hot ISM of galaxies could be important X-ray sources as well (Mineo, Gilfanov & Sunyaev 2012a; Pacucci et al. 2014). In principle, our approach could couple detailed spectral models, composed of X-ray emission from a variety of sources, to the properties of the IGM with time, and investigate how the details of population synthesis models, for example, manifest themselves in the global 21-cm signal. Such studies would be particularly powerful if partnered with models of the 21-cm angular power spectrum, observations of which could help break SED-related degeneracies (Pritchard & Furlanetto 2007; Mesinger et al. 2013; Pacucci et al. 2014).

5.5 Helium effects

The $x_{\mathrm{H\,I}} = x_{\mathrm{He\,I}}$ approximation we have made throughout is common in the literature, and has been validated to some extent by the close match in H I and He I global ionization histories computed in Wyithe & Loeb (2003) and Friedrich et al. (2012), for example. However, recent studies of the ionization profiles around stars and quasars (e.g. Thomas & Zaroubi 2008; Venkatesan & Benson 2011) find that more X-ray luminous galaxies have larger He I regions than H II regions. Given that the metagalactic radiation field we consider in this work is even harder than the quasar-like spectra considered in the aforementioned studies, the H I and He I fractions in the bulk IGM may differ even more substantially than they do in the outskirts of H II/He I regions near quasars.

We have neglected a self-consistent treatment of helium in this work, though more detailed calculations including helium could have a substantial impact on the ionization and thermal history. Ciardi, Bolton & Maselli (2012) showed that radiative transfer simulations including helium, relative to their hydrogen-only counterparts, displayed a slight delay in the redshift of reionization, since a small fraction of energetic photons are absorbed by helium instead of hydrogen. The simulations including helium also exhibited an increase in the IGM temperature at $z \lesssim 10$ due to helium photoheating. At $z \gtrsim 10$, the volume-averaged temperature in the hydrogen-only simulations was actually larger due to the larger volume of ionized gas. It is difficult to compare such results directly to our own, as our interest lies in the IGM temperature *outside* of ionized regions. Because of this complication, we defer a more detailed investigation of helium effects to future work.

6 CONCLUSIONS

Our conclusions can be summarized as follows.

(i) Approximate solutions to the cosmological RTE overestimate the heating rate density in the bulk IGM, leading to artificially shallower absorption features in the global 21-cm signal, perhaps by $\sim$15−20 mK if sources with hard spectra dominate the X-ray background (Fig. 3).

(ii) Brute-force solutions are computationally expensive, which limits parameter space searches considerably. The discretization scheme of Haardt & Madau (1996) is fast, though exquisite redshift sampling is required in order to accurately model X-ray heating (Fig. 2).

(iii) More realistic X-ray spectra are harder than often used power-law treatments (Fig. 4), and thus lead to deeper absorption features in the global 21-cm signal at fixed bolometric luminosity density. While the details of coronal physics can harden a 'pure MCD' spectrum enough to modify the global 21-cm absorption feature at the $\sim$10 mK level (in the extreme case of $f_{\mathrm{sc}} = 1$ and $\alpha = -0.5$), the characteristic mass of accreting BHs (amount of neutral absorption in galaxies) has an even more noticeable impact, shifting the absorption trough in amplitude by $\sim$20 ($\sim$ 50) mK and in redshift by $\Delta z \approx 0.5$ ($\Delta z \approx 2$) (Fig. 5).

(iv) Care must be taken when using the local L_{X}−SFR relation to draw inferences about the high-z stellar IMF, as assumptions about source SEDs are built-in to the often used normalization factor f_{X}. Even if the high-z X-ray background is dominated by X-ray binaries, the parameters governing how significantly the intrinsic disc emission is processed influence the signal enormously, and could vary significantly from galaxy to galaxy.

Though our code was developed to study the global 21-cm signal, it can be used as a stand-alone radiation background calculator, whose output could be easily integrated into cosmological simulation codes to investigate large-scale feedback. It is publicly available,[6] and remains under active development.

ACKNOWLEDGEMENTS

JM would like to thank Greg Salvesen, Jack Burns, Steven Furlanetto, Andrei Mesinger, and John Wise for thoughtful discussions and comments on an earlier version of this manuscript, Stephen Murray for developing the HMF-CALC code (Murray et al. 2013) and being so responsive to questions regarding its use, and the anonymous referee for providing a thorough review that helped improve the quality of this paper. JM acknowledges partial funding from The LUNAR consortium (http://lunar.colorado.edu), headquartered at the University of Colorado, which is funded by the NASA Lunar Science Institute (via Cooperative Agreement NNA09DB30A) to investigate concepts for astrophysical observatories on the Moon. This work used the `JANUS` supercomputer, which is supported by the National Science Foundation (award number CNS-0821794) and the University of Colorado Boulder. The `JANUS` supercomputer is a joint effort of the University of Colorado Boulder, the University of Colorado Denver, and the National Center for Atmospheric Research. This work also made use of PYTHON, including the packages NUMPY, MATPLOTLIB, H5PY, and SCIPY.

[6] https://bitbucket.org/mirochaj/glorb

REFERENCES

Abel T., Bryan G. L., Norman M. L., 2002, Sci, 295, 93
Bardeen J. M., 1970, Nature, 226, 64
Barkana R., Loeb A., 2001, Phys. Rep., 349, 125
Barkana R., Loeb A., 2005, ApJ, 626, 1
Basu-Zych A. R. et al., 2013, ApJ, 762, 45
Begelman M. C., Volonteri M., Rees M. J., 2006, MNRAS, 370, 289
Belczynski K., Kalogera V., Rasio F. A., Taam R. E., Zezas A., Bulik T., Maccarone T. J., Ivanova N., 2008, ApJS, 174, 223
Benson A., Venkatesan A., Shull J. M., 2013, ApJ, 770, 76
Bromm V., Coppi P. S., Larson R. B., 1999, ApJ, 527, L5
Bromm V., Kudritzki R. P., Loeb A., 2001, ApJ, 552, 464
Bromm V., Yoshida N., Hernquist L., McKee C F., 2009, Nature, 459, 49
Brorby M., Kaaret P., Prestwich A., 2014, MNRAS, 441, 2346
Burns J. O. et al., 2012, Adv. Space Res., 49, 433
Chen X., Miralda-Escudé J., 2004, ApJ, 602, 1
Chuzhoy L., Alvarez M. A., Shapiro P. R., 2006, ApJ, 648, L1
Ciardi B., Salvaterra R., Di Matteo T., 2010, MNRAS, 401, 2635
Ciardi B., Bolton J. S., Maselli A., 2012, MNRAS, 423, 558
Davies F. B., Furlanetto S. R., 2014, MNRAS, 437, 1141
Dijkstra M., Gilfanov M., Loeb A., Sunyaev R., 2012, MNRAS, 421, 213
Fabbiano G., 2006, ARA&A, 44, 323
Fialkov A., Barkana R., Visbal E., 2014, Nature, 506, 197
Field G. B., 1958, Proc. IRE, 46, 240
Fragos T., Lehmer B. D., Naoz S., Zezas A., Basu-Zych A., 2013, ApJ, 776, L31
Friedrich M. M., Mellema G., Iliev I. T., Shapiro P. R., 2012, MNRAS, 421, 2232
Fukugita M., Kawasaki M., 1994, MNRAS, 269, 563
Furlanetto S. R., 2006, MNRAS, 371, 867
Furlanetto S. R., Loeb A., 2004, ApJ, 611, 642
Furlanetto S. R., Pritchard J. R., 2006, MNRAS, 372, 1093
Furlanetto S. R., Stoever S. J., 2010, MNRAS, 404, 1869
Furlanetto S. R., Oh S. P., Briggs F. H., 2006, Phys. Rep., 433, 181
Gilfanov M., Grimm H.-J., Sunyaev R., 2004, MNRAS, 347, L57
Gnedin N. Y., Kravtsov A. V., Chen H. W., 2008, ApJ, 672, 765
Greenhill L. J., Bernardi G., 2012, in Komonjinda S., Kovalev Y., Ruffolo D., eds, Invited review to the 11th Asian-Pacific Regional IAU Meeting 2011, NARIT Conf. Ser., 1, preprint (arXiv:1201.1700)
Greiner J. et al., 2009, ApJ, 693, 1610
Grimm H.-J., Gilfanov M., Sunyaev R., 2003, MNRAS, 339, 793
Haardt F., Madau P., 1996, ApJ, 461, 20
Haiman Z., Loeb A., 1998, ApJ, 503, 505
Haiman Z., Rees M. J., Loeb A., 1997, ApJ, 476, 458
Haiman Z., Abel T., Rees M. J., 2000, ApJ, 534, 11
Harker G. J. A., Pritchard J. R., Burns J. O., Bowman J. D., 2012, MNRAS, 419, 1070
Hirata C. M., 2006, MNRAS, 367, 259
Jeon M., Pawlik A. H., Bromm V., Milosavljević M., 2014, MNRAS, 440, 3778
Kaaret P., 2014, MNRAS, 440, L26
Kaaret P., Schmitt J., Gorski M., 2011, ApJ, 741, 10
King A. R., Kolb U., 1999, MNRAS, 305, 654
Komatsu E. et al., 2011, ApJS, 192, 18
Kuhlen M., Madau P., 2005, MNRAS, 363, 1069
Lewis A., Challinor A., Lasenby A., 2000, ApJ, 538, 473
Linden T., Kalogera V., Sepinsky J. F., Prestwich A., Zezas A., Gallagher J. S., 2010, ApJ, 725, 1984
Mcquinn M., 2012, MNRAS, 426, 1349
Madau P., Meiksin A., Rees M. J., 1997, ApJ, 475, 429
Madau P., Rees M. J., Volonteri M., Haardt F., Oh S. P., 2004, ApJ, 604, 484
Mapelli M., Ripamonti E., Zampieri L., Colpi M., Bressan A., 2010, MNRAS, 408, 234
Meiksin A., White M., 2003, MNRAS, 342, 1205
Mesinger A., Furlanetto S., 2009, MNRAS, 400, 1461
Mesinger A., Bryan G. L., Haiman Z., 2009, MNRAS, 399, 1650
Mesinger A., Furlanetto S., Cen R., 2011, MNRAS, 411, 955
Mesinger A., Ferrara A., Spiegel D. S., 2013, MNRAS, 431, 621
Miller J. M., Cackett E. M., Reis R. C., 2009, ApJ, 707, L77
Mineo S., Gilfanov M., Sunyaev R., 2012a, MNRAS, 426, 1870
Mineo S., Gilfanov M., Sunyaev R., 2012b, MNRAS, 419, 2095
Mirabel I. F., Dijkstra M., Laurent P., Loeb A., Pritchard J. R., 2011, A&A, 528, A149
Mirocha J., Skory S., Burns J. O., Wise J. H., 2012, ApJ, 756, 94
Mirocha J., Harker G. J. A., Burns J. O., 2013, ApJ, 777, 118
Mitsuda K. et al., 1984, PASJ, 36, 741
Murray S. G., Power C., Robotham A. S. G., 2013, Astron. Comput., 3, 23
Oh S. P., 2001, ApJ, 553, 499
Pacucci F., Mesinger A., Mineo S., Ferrara A., 2014, MNRAS, preprint (arXiv:1403.6125)
Parsons A. R. et al., 2014, ApJ, 788, 106
Power C., James G., Combet C., Wynn G., 2013, ApJ, 764, 76
Press W. H., Schechter P., 1974, ApJ, 187, 425
Prestwich A. H., Tsantaki M., Zezas A., Jackson F., Roberts T. P., Foltz R., Linden T., Kalogera V., 2013, ApJ, 769, 92
Pritchard J. R., Furlanetto S. R., 2006, MNRAS, 367, 1057
Pritchard J. R., Furlanetto S. R., 2007, MNRAS, 376, 1680
Pritchard J. R., Loeb A., 2012, Rep. Prog. Phys., 75, 086901
Ranalli P., Comastri A., Setti G., 2003, A&A, 399, 39
Ricotti M., Ostriker J. P., 2004, MNRAS, 352, 547
Ripamonti E., Mapelli M., Zaroubi S., 2008, MNRAS, 387, 158
Santos M. G., Ferramacho L., Silva M. B., Amblard A., Cooray A., 2010, MNRAS, 406, 2421
Schaerer D., 2002, A&A, 382, 28
Shakura N. I., Sunyaev R. A., 1973, A&A, 24, 337
Shapiro S. L., Lightman A. P., Eardley D. M., 1976, ApJ, 204, 187
Shull J. M., van Steenberg M. E., 1985, ApJ, 298, 268
Steiner J. F., Narayan R., McClintock J. E., Ebisawa K., 2009, PASP, 121, 1279
Tanaka T., Perna R., Haiman Z., 2012, MNRAS, 425, 2974
Thomas R. M., Zaroubi S., 2008, MNRAS, 384, 1080
Totani T., Kawai N., Kosugi G., Aoki K., Yamada T., Iye M., Ohta K., Hattori T., 2006, PASJ, 58, 485
Tumlinson J., Shull J. M., Venkatesan A., 2003, ApJ, 584, 608
Venkatesan A., Benson A., 2011, MNRAS, 417, 2264
Venkatesan A., Giroux M. L., Shull J. M., 2001, ApJ, 563, 1
Verner D. A., Ferland G. J., 1996, ApJS, 103, 467
Volonteri M., Madau P., Quataert E., Rees M. J., 2005, ApJ, 620, 69
Voytek T. C., Natarajan A., Jáuregui García J. M., Peterson J. B., López-Cruz O., 2014, ApJ, 782, L9
Wise J. H., Cen R., 2009, ApJ, 693, 984
Wolcott-Green J., Haiman Z., 2012, MNRAS, 425, L51
Wouthuysen S. A., 1952, AJ, 57, 31
Wyithe J. S. B., Loeb A., 2003, ApJ, 586, 693
Zygelman B., 2005, ApJ, 622, 1356

APPENDIX A: ANALYTIC TEST PROBLEM

In this section, we test our code with a double power-law form for the X-ray emissivity, $\hat{\epsilon}_\nu(z) \propto (1+z)^\beta \nu^{\alpha-1}$, noted by Meiksin & White (2003) to yield analytic solutions in two important limiting cases. In the optically thin limit (e.g. the cosmologically limited, CL, case of Meiksin & White 2003, in which $\overline{x}_i = 1$ at all redshifts), we find

$$\widehat{J}_{\nu,\mathrm{CL}}(z) = \frac{c}{4\pi}\frac{\hat{\epsilon}_\nu(z)}{H(z)}\frac{(1+z)^{9/2-(\alpha+\beta)}}{\alpha+\beta-3/2} \times \left[(1+z_{\mathrm{f}})^{\alpha+\beta-3/2} - (1+z)^{\alpha+\beta-3/2}\right]. \quad \text{(A1)}$$

In the Lyα literature, it is common to accommodate the alternative 'absorption-limited' (AL) case in which $\overline{\tau}_\nu > 0$, by defining the 'attenuation length', r_0, as $\exp[-\tau_\nu(z,z')] \equiv \exp[-l_H(z,z')/r_0]$, where l_H is the proper distance between redshifts z and z'. Instead, we will adopt the neutral-medium approximation of equation (20) (i.e. $\overline{x}_i = 0$), which permits the partially analytic solution

$$\widehat{J}_{\nu,\mathrm{AL}}(z) = \frac{c}{4\pi}\frac{\hat{\epsilon}_\nu(z)}{H(z)}(1+z)^{9/2-(\alpha+\beta)} \times \exp\left[-\left(\frac{\mu}{\nu}\right)^3 (1+z)^{3/2}\right]\mathcal{A}_\nu(\alpha,\beta,z,z_\mathrm{f}) \tag{A2}$$

with

$$\mathcal{A}_\nu \equiv \int_{z'=z}^{z'=z_\mathrm{f}} (1+z')^{\alpha+\beta-5/2}\exp\left[\left(\frac{\mu}{\nu}\right)^3 \frac{(1+z)^3}{(1+z')^{3/2}}\right]\mathrm{d}z'. \tag{A3}$$

The function A_ν has analytic solutions (in the form of exponential integrals) only for $\alpha+\beta = 3n/2$ where n is a positive integer, which represents physically unrealistic scenarios.

The metagalactic spectral index in this case works out to be

$$\alpha_\mathrm{MG} \equiv \frac{\mathrm{d}\log J_\nu}{\mathrm{d}\log\nu} = \alpha + 3\left(\frac{\mu}{\nu}\right)^3 (1+z)^{3/2}\left[1-\mathcal{B}_\nu(1+z)^{3/2}\right], \tag{A4}$$

where

$$\mathcal{B}_\nu = \mathcal{A}_\nu^{-1}\int_z^{z_\mathrm{f}} (1+z')^{\alpha+\beta-4}\exp\left[\left(\frac{\mu}{\nu}\right)^3 \frac{(1+z)^3}{(1+z')^{3/2}}\right]\mathrm{d}z'. \tag{A5}$$

As $\nu \to \infty$, the second term vanishes, leaving the optically thin limit, $\alpha_\mathrm{MG} = \alpha$. As $\nu \to 0$, $\mathcal{B}_\nu \to 0$, meaning $\alpha_\mathrm{MG} = \alpha + 3$. The 'break' in the cosmic X-ray background spectrum occurs when $\alpha_\mathrm{MG} = 0$, corresponding to a photon energy of

$$h\nu_* = h\mu(1+z)\left\{\frac{3}{\alpha}\left[\mathcal{B}_{\nu_*} - (1+z)^{-3/2}\right]\right\}^{1/3} \tag{A6}$$

which must be solved iteratively. Solutions are presented in Fig. A1 for $\alpha = -1.5$, $\beta = -3$, $\hat{\epsilon}_\nu(z_0) = 10^{-2}$ for $z_0 = 10$, $z_\mathrm{f} = 15$, and show good agreement between analytic and numerical solutions.

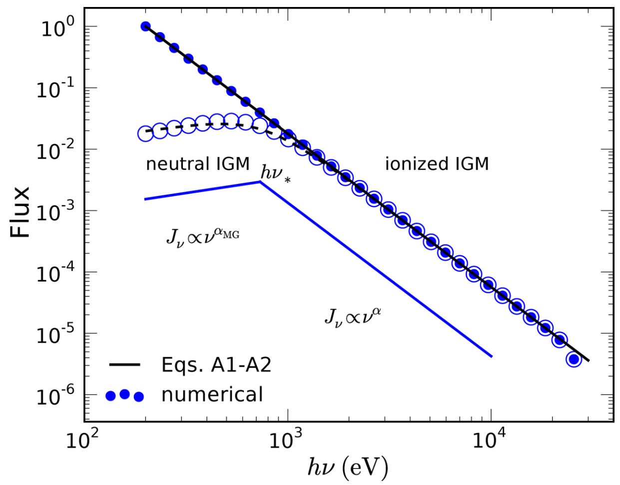

Figure A1. Cosmic X-ray background spectrum at $z = 20$ for $\alpha = -1.5$ and $\beta = -3$. Normalization of the y-axis can be scaled arbitrarily depending on the normalization of the emissivity. The deviation at high energies is due to the fact that the analytic solution is not truncated by z_f or E_max, meaning there are always higher energy photons redshifting to energies $h\nu \le h\nu_\mathrm{max}$. The numerical solutions are computed with finite integration limits and truncated at E_max, such that the emissivity at $h\nu > h\nu_\mathrm{max}$ is zero, resulting in no flux at $h\nu \ge h\nu_\mathrm{max}$. Elsewhere, the agreement is very good, with discrepancies arising solely due to the use of approximate bound-free photoionization cross-sections in the analytic solution.

This paper has been typeset from a TEX/LATEX file prepared by the author.